Developing a new mathematical model and evaluation of the effect of parabolic mirror edge rounding on the collimated field quality of an infrared collimator used in single-channel aerial vehicle testing equipment

Tran Quoc Huy*, Do Anh Cuong, Pham Duc Thong, Pham Van May

Institute of Missile, Academy of Military Science and Technology, 17 Hoang Sam, Nghia Do, Hanoi, Vietnam.

*Corresponding author: tranhuyvtl@gmail.com

Received 10 Jan. 2026; Revised 20 May 2026; Accepted 21 May 2026; Published 25 Aug. 2026.

DOI: https://doi.org/10.54939/1859-1043.j.mst.113.2026.30-37

ABSTRACT

Parabolic-mirror infrared (IR) collimators are widely used in single-channel flight vehicle testing to generate quasi-plane-wave radiation fields. However, edge diffraction degrades field uniformity and limits measurement accuracy. This paper presents a mathematical model of an IR collimator with rounded mirror edges to evaluate their influence on the radiation field. The model is formulated using the two-dimensional Helmholtz equation and solved by the boundary integral equation method to determine the induced surface current and the resulting radiation field. Numerical results demonstrate that rounded edges effectively suppress diffraction-induced amplitude ripples and improve field uniformity compared with conventional sharp-edge mirrors. The proposed model provides a theoretical basis for optimizing parabolic IR collimators for high-accuracy flight vehicle testing.

Keywords: Infrared collimator; Parabolic mirror; Rounded edges; Edge diffraction; Single-channel aerial vehicle.

1. INTRODUCTION

Parabolic-mirror infrared (IR) collimators are key components of high-precision single-channel test systems for generating a nearly planar wavefield. However, diffraction caused by the mirror's finite aperture and edge geometry introduces field non-uniformity, reducing calibration accuracy and measurement repeatability.

Diffraction phenomena at the edges of finite-aperture reflectors have been studied extensively. In the RF/microwave regime, numerous studies on compact antenna test ranges (CATRs) have analyzed the formation of quiet zones, evaluated field quality, and investigated methods for edge treatment of reflectors [1–3]. Recent studies have shown that smoothly blended elliptical edges with continuous junctions are significantly more effective than sharp-edged truncations [7]. In the infrared regime, off-axis parabolic mirrors (OAPs) remain widely used as collimating elements [4–6] and continue to be investigated in terms of diffraction-limited performance [9]. Current modeling approaches include asymptotic methods such as GO, PO, GTD, UTD, and PTD, which have recently been extended through accelerated ray-tracing techniques [10], as well as full-wave methods such as the boundary integral equation (BIE) method and the method of moments (MoM) for analyzing the sensitivity of collimator-field quality to reflector shape and edge geometry [8], [11]. Recent advances in MWIR zoom optics and compact relay optical systems have significantly improved infrared imaging performance [14, 15]. Nevertheless, these studies assume an ideal incident wavefront and do not address the effect of parabolic mirror edge diffraction on collimated field quality, which is investigated in this work. However, when the edge radius of curvature is on the order of the operating wavelength, asymptotic models lose accuracy and must be replaced by full-wave formulations.

Despite these studies, the quantitative relationship between parabolic-mirror edge geometry and the field quality of infrared collimators has not been fully established using rigorous full-wave analysis. This paper addresses this gap by developing a BIE model of a parabolic mirror with a smoothly rounded elliptical edge and slope continuity, and quantitatively evaluating its effects on field uniformity and wavefront quality in a representative (LWIR) configuration.

2. MATHEMATICAL MODEL

2.1. Problem formulation and assumptions

The infrared collimator considered in this study employs a finite-aperture parabolic mirror with rounded edges, as shown in Figure 1, to generate a nearly planar wavefield within a predefined working region. Because the system exhibits translational invariance along the vertical axis, the problem is formulated in a two-dimensional Cartesian coordinate system *(x, y)*.

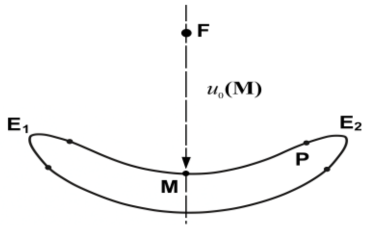

Figure 1. *Geometry of the parabolic mirror with rounded edges.*

This 2D model provides a reasonable approximation for two practical cases. The first is a parabolic cylindrical reflector combined with a line source, for which translational invariance is strictly preserved. The second is the meridional-plane analysis of an axially symmetric paraboloid, in which the edge-rounding mechanism - namely, the local smoothing of the induced-current singularity at the mirror rim - can still be described reasonably well by the cross-sectional model, especially for observation regions on or near the axis, as commonly encountered in single-channel probe experiments. Extension to the full three-dimensional rotational problem will be addressed in future work.

The mirror is modeled as an ideal parabolic surface described by:

$$y = \frac{x^2}{4f} \tag{1}$$

where f denotes the focal length of the parabolic mirror. The infrared source is located at the focal point of the parabola, ensuring ideal collimation in the absence of diffraction.

To reduce diffraction caused by abrupt truncation of the parabolic surface, the mirror edges are smoothly rounded. Each rounded edge is described by a general second-order curve of elliptical type E_1, E_2:

$$\frac{\left(x - x_c\right)^2}{a^2} + \frac{\left(y - y_c\right)^2}{b^2} = 1 \tag{2}$$

where (x_c, y_c) is the ellipse center and *a, b* are the semi-axes along the aperture and longitudinal directions, respectively. The characteristic rounding dimension reported in Section 3.1 is defined as $L_r \equiv a$. At the junction point (x_0, y_0) = (a_p, $a_p^2/4f$), two continuity conditions are enforced: position continuity (the ellipse passes through (x_0, y_0)) and slope continuity ($(dy/dx)_{ellipse}$ = $(dy/dx)_{parabola} = x_0/(2f)$ at the junction). These two conditions uniquely determine the ellipse center (x_c, y_c) once (*a, b*) are chosen. The slope-continuity condition is essential - without it, a residual corner at the junction would itself act as a diffraction source and partially defeat the purpose of edge rounding.

The complete mirror contour, denoted by *C*. In Figure 1, *M* is the observation point on the conducting surface, is a secondary source point running along the mirror contour *C* and associated with the induced current density *J(P)*, and the incident field $u_o(M)$ is generated by a primary source located at the focal point *F*, which only contributes to the incident field and does not belong to the integration contour.

2.2. Governing equations and boundary conditions

The electromagnetic field is assumed to be time-harmonic with angular frequency ω. Using a scalar Borgnis function *u(x,y)*, The free-space field satisfies the 2D Helmholtz equation [13]:

$$\nabla^2 u + k^2 u = f(r) \tag{3}$$

where $k = 2\pi/\lambda$ is the wavenumber corresponding to the infrared wavelength λ, and $f(r)$ denotes the excitation from the IR source at the parabolic-mirror focus.

The parabolic mirror is assumed to be a perfect electric conductor (PEC). The PEC idealization is quantitatively well-supported for IR-band reflectors with standard metallic coatings. At the working wavelength λ = 10.6 µm, the complex relative permittivity of Au/Al is approximately $\varepsilon_r \approx -8000 + j2000$, with gold giving comparable values; this corresponds to a surface impedance of magnitude $|Z_s| \approx 0.03\ \Omega$ — more than four orders of magnitude below the free-space wave impedance $\eta_o \approx 377\ \Omega$. The resulting insertion loss is confined to 0.02 – 0.04 dB and the local phase shift relative to the ideal PEC reference is below 0.01°. These finite-conductivity corrections are negligibly small compared with the percent-level amplitude non-uniformities and degree-level phase deviations introduced by edge rounding, so the PEC assumption introduces no observable bias in the comparative metrics reported here. Consequently, for the transverse magnetic (TM) polarization considered in this study, the Dirichlet boundary condition on the mirror contour *C* is

$$u|_C = 0 \tag{4}$$

The scattered field satisfies the Sommerfeld radiation condition at infinity [12]:

$$\left(\frac{\partial u}{\partial r} + iku\right)_{r\to\infty} = o\left(\frac{1}{\sqrt{r}}\right) \tag{5}$$

which ensures that only outward-propagating waves are present.

2.3. Electromagnetic field components

For the TM polarization, the electromagnetic field components are expressed in terms of the scalar function *u(x,y)* as

$$E_x = -\frac{i}{\omega\varepsilon}\frac{\partial u}{\partial y}, E_y = \frac{i}{\omega\varepsilon}\frac{\partial u}{\partial x} \tag{6}$$

$$E_z = H_x = H_y = 0, H_z = u(x,y) \tag{7}$$

Thus, once the function *u(x,y)* is determined, the complete electromagnetic field distribution in the working region of the parabolic mirror collimator can be readily obtained.

2.4. Green's function and boundary integral representation

The Green's function for the 2D Helmholtz equation [13] is given by:

$$\nabla^2 g(M,P) + k^2 g(M,P) = -2\pi\delta|\mathrm{r}_M - \mathrm{r}_P| \tag{8}$$

with the solution

$$g(M,P) = -\frac{i\pi}{2}H_0^{(2)}\left(k|\mathrm{r}_M - \mathrm{r}_P|\right) \tag{9}$$

where $H_0^{(2)}(\bullet)$ denotes the zero-order Hankel function of the second kind.

The total field is written as $u = u_0 + u_s$, where u_0 is the incident field produced by the source and u_s is the scattered field. Introducing the unknown boundary function

$$J(P) \triangleq \frac{\partial u(P)}{\partial n}, \qquad P \in C \tag{10}$$

and applying Green's second identity together with the PEC boundary condition, the scattering problem is reduced to the following boundary integral equation on the mirror contour:

$$H_0^{(2)}(kr_M) = -\frac{1}{2\pi} \oint_C J(P) H_0^{(2)}\left(k\left|\mathrm{r}_M - \mathrm{r}_P\right|\right) ds, \qquad M \in C \tag{11}$$

2.5. Discretization and linear system

The contour C of the parabolic mirror is divided into N small boundary elements C_n of length Δ_n. Assuming *J(P)* to be constant over each element $J(P) \approx J_n$ for $P \in C_n$ and enforcing Equation (11) at collocation points $M_m \in C$, the result is discretized as

$$H_0^{(2)}(kr_m) = -\frac{1}{2\pi} \sum_{n=1}^{N} J_n \int_{C_n} H_0^{(2)}\left(k\left|\mathrm{r}_m - \mathrm{r}_P\right|\right) ds, \qquad m = 1, 2, ..., N \tag{12}$$

Defining the interaction coefficients

$$M_{m,n} = -\frac{1}{2\pi} \int_{C_n} H_0^{(2)}\left(k\left|\mathrm{r}_m - \mathrm{r}_P\right|\right) ds \tag{13}$$

equation (12) is transformed into a linear system.

For $(m \neq n)$, the kernel is smooth and the integral is approximated by the midpoint rule:

$$M_{m,n} = -\frac{\Delta_n}{2\pi} H_0^{(2)}\left(\sqrt[k]{(x_m - x_n)^2 + (y_m - y_n)^2}\right), \qquad m \neq n \tag{14}$$

For the diagonal terms $(m = n)$, the Hankel kernel exhibits a logarithmic singularity. Following the analytical treatment used in the reference paper, the diagonal element is given by

$$M_{m,n} = -\frac{\Delta_n}{\pi}\left[1 - i\frac{2}{\pi}\ln\left(\frac{\gamma k \Delta_n}{4e}\right)\right], \tag{15}$$

where γ is the Euler constant and e is the base of the natural logarithm. This term is essential for ensuring numerical stability and accuracy.

Using (13)–(15), the discretized boundary integral equation becomes:

$$\sum_{n=1}^{N} M_{m,n} J_n = H_0^{(2)}(kr_m), \qquad m = 1, 2, ..., N. \tag{16}$$

2.6. Field computation in the working region

Once the induced surface current distribution is known, the field at any observation point M in the working region is computed by the radiation integral

$$H_z(M) = \frac{1}{2\pi} \oint_C J(P) H_0^{(2)}\left(k\left|\mathrm{r}_M - \mathrm{r}_P\right|\right) ds \tag{17}$$

which, in discretized form, becomes

$$H_z(M) \approx \frac{1}{2\pi} \sum_{n=1}^{N} J_n H_0^{(2)}(kr_{n,M}) \Delta_n \tag{18}$$

where $r_{n,M}$ denotes the distance between the observation point and the center of the n-th boundary element. This expression provides the basis for the quantitative evaluation of field amplitude and uniformity in the working region of the parabolic mirror collimator.

The proposed full-wave electromagnetic model describes diffraction from the finite aperture and rounded edges of a parabolic mirror, enabling a quantitative evaluation of their influence on the collimated infrared field.

3. NUMERICAL RESULTS AND QUANTITATIVE ANALYSIS

3.1. Simulation setup

Numerical simulations were carried out based on the mathematical model developed in Section 2. The complete set of simulation parameters is summarized in Table 1.

Table 1. *Simulation parameters for the LWIR case study.*

No.	Parameter	Symbol	Unit	Value
1	Wavelength (LWIR)	λ	μm	10.6
2	Mirror diameter	D	mm	150
3	Focal length	f	mm	250
4	Half-aperture (parabolic segment)	a_p	mm	75
5	Edge rounding - sharp	L_r	μm	5.3 (≈ 0.5 λ)
6	Edge rounding - small	L_r	μm	10.6 (≈ 1.0 λ)
7	Edge rounding - large	L_r	μm	15.9 (≈ 1.5 λ)
8	Discretization density	NPW	elements / λ	30
9	Observation distance (axial)	z_0	mm	500

The parabolic contour was discretized into uniformly distributed boundary elements at a density of NPW = 30 elements per wavelength, with a local refinement factor of 1.7 times in the rounded-edge regions to resolve the local geometry. A convergence study verified that the non-uniformity metric δ converges to within 0.5% of its asymptotic value for NPW ≥ 25. The chosen NPW = 30 therefore lies safely within the converged regime. The singular diagonal terms of the boundary integral system are evaluated using the analytical expression (15), and the resulting linear system is solved directly. Once the induced surface current J(M) is obtained, the field in the working region is computed using the radiation integral (18).

To characterize the collimation quality, four quantitative metrics are defined over the working region:

+ amplitude non-uniformity: $\delta = (|H|_{max} - |H|_{min})/\langle|H|\rangle$;
+ amplitude RMS ripple: $\sigma_{amp} = \mathrm{std}(|H|)/\langle|H|\rangle$;
+ phase peak-to-valley: $PV_\varphi = \max[\Delta\varphi(x)] - \min[\Delta\varphi(x)]$;
+ RMS wavefront error: $WFE_{RMS} = \mathrm{std}[\Delta\varphi]/(2\pi)$, in units of λ.

where Δφ(x) is the phase deviation from an ideal planar reference and the operators max, min, std(·), and ⟨·⟩ act over the working region.

Figure 2a shows the magnitude of the induced current $|J(s)|$ along the mirror contour. For the sharp-edge configuration, strong current concentrations are observed at the mirror extremities, characteristic of edge singularities and acting as intense secondary sources of diffraction. Rounded edges progressively suppress these concentrations and yield smoother current distributions, with the suppression strength increasing with L_r. Figure 2b shows the corresponding transverse distribution of the normalized magnetic field amplitude $|H_z|/|H_z|_{max}$ in the working region. The sharp-edge case exhibits pronounced amplitude ripples caused by edge-diffraction-induced interference; both rounded configurations significantly reduce the ripple amplitude.

The collimation-quality metrics for all three configurations are summarized in Table 2. The large rounded edge reduces δ by approximately 56% and WFE_{RMS} by approximately 59% relative to the sharp-edge baseline, demonstrating that edge shaping has a strong and quantifiable influence on both the amplitude uniformity and the wavefront quality of the collimated IR field.

Table 2. *Collimation-quality metrics for the three edge configurations.*

No.	Configuration	δ (%)	σ_{amp} (%)	PV_{φ} (°)	WFE_{RMS} (λ)
1	Sharp edge (L_r = 0.5)	12.3	4.1	18.5	0.029
2	Small rounding ($L_r \approx 1.0\lambda$)	7.6	2.5	11.2	0.018
3	Large rounding ($L_r \approx 1.5\lambda$)	5.4	1.7	7.8	0.012
4	Improvement (large vs sharp)	−56%	−59%	−58%	−59%

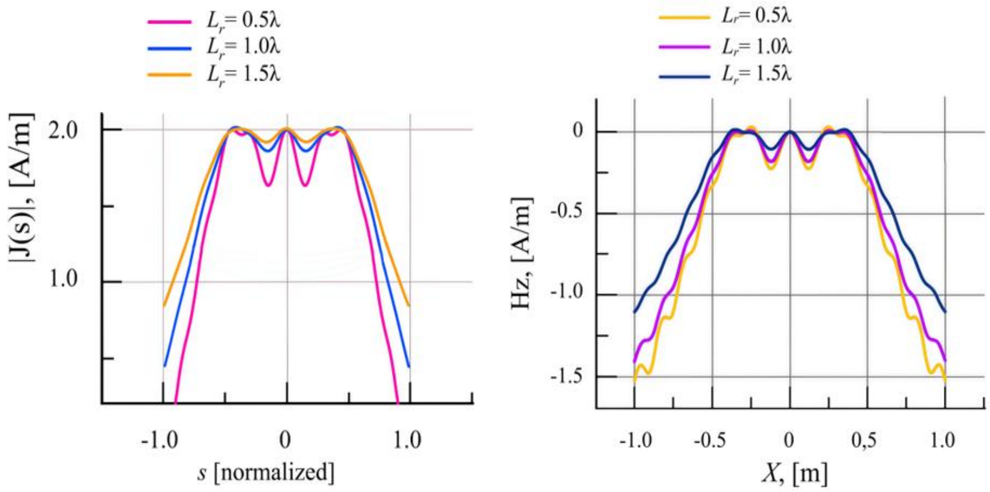

a) *b)*

Figure 2. *Numerical results for three edge configurations of the parabolic-mirror IR collimator a) Magnitude of the induced surface current |J(s)| along the mirror contour; b) Transverse distribution of the normalized magnetic field amplitude H_z in the working region.*

3.2. Discussion

The results show that diffraction at the mirror edge is the dominant mechanism degrading the field quality of infrared collimators based on finite-aperture parabolic mirrors. Smooth edge rounding with continuous slope at the transition region provides an effective geometric solution for mitigating this effect. The main improvement mechanism lies in reducing the induced-current singularity at the mirror rim and smoothing the transition at the aperture boundary.

At the system-level perspective, wavefront error directly affects experimental quality. For a single-channel infrared seeker, the RMS wavefront error across the working aperture, WFE_{RMS}, corresponds to an apparent angular error of approximately $2\pi \cdot WFE_{RMS}/(kD)$, which manifests as a virtual target-position displacement perceived by the seeker. In experiments requiring sub-milliradian angular accuracy, wavefront error is often the dominant collimator-induced error source, outweighing the influence of amplitude non-uniformity. The proposed model therefore enables simultaneous evaluation of both metrics within a unified framework, thereby facilitating collimator assessment against system-level performance indicators.

From a manufacturing perspective, this solution is entirely feasible. At $\lambda = 10.6\mu m$, the required edge-rounding size in the range of 5–20μm is well within the capability of modern infrared mirror fabrication technologies, especially single-point diamond turning, with form accuracy below 100 nm, and magnetorheological finishing, with sub-10 nm precision. For a mirror diameter of 150 mm, the relative ratio $L_r/D \approx 10^{-4}$ is comparable to the level commonly encountered in standard astronomical infrared optics. Furthermore, typical manufacturing tolerances of approximately ±1 μm in L_r introduce a variation in field non-uniformity of less than 1%, and therefore do not alter the fundamental design conclusions.

The rounded-edge solution also involves a small trade-off in effective aperture. Because the rounded section replaces the outermost region of the parabolic surface, the effective collimating aperture decreases from D to $D'=D - 2L_r$. However, in a representative LWIR case, the relative aperture loss is only about $2L_r/D \approx 0.03\%$, which is negligible compared with the 50–60% improvement in field uniformity. Under the design rule $L_r \sim \lambda$, the aperture loss remains below 0.02% for large IR collimators ($D \gg 10^3\lambda$), so rounded edges are clearly advantageous in this regime. Only for miniature systems with $D \sim 10^2\lambda$, which are uncommon in the infrared band but may occur in the sub-millimeter or THz range, does this trade-off require separate evaluation.

From a design standpoint, choosing the edge-rounding dimension on the order of the operating wavelength is a practical and well-balanced solution, since it significantly improves both amplitude uniformity and wavefront quality while causing negligible loss of effective aperture and remaining fully compatible with existing fabrication capabilities. The proposed BIE model enables these trade-offs to be quantified systematically, thereby supporting the design and optimization of parabolic-mirror infrared collimators for high-precision testing of single-channel flight vehicles.

4. CONCLUSIONS

This paper investigated the influence of rounded edges on the collimated field quality of a parabolic-mirror infrared collimator. A full-wave electromagnetic model based on the two-dimensional Helmholtz equation and the boundary integral equation (BIE) method was employed to analyze edge-diffraction effects caused by the finite mirror aperture. The results confirm that edge diffraction is the primary factor limiting field uniformity. Compared with conventional sharp edges, properly designed rounded edges effectively suppress diffraction-induced amplitude ripples and improve field uniformity within the working region. The degree of improvement depends on the rounded-edge geometry.

The present analysis is limited to a 2D formulation with a perfect-electric-conductor approximation of the mirror surface. Although the qualitative conclusions are expected to remain valid for 3D axisymmetric geometries and realistic Al/Au coatings, quantitative refinement requires further model development. Future work will extend the approach to a full 3D body-of-revolution Method-of-Moments formulation, incorporate impedance boundary conditions for realistic IR coatings, and perform experimental validation using IR-camera field mapping, LWIR wavefront sensing, and comparison with a commercial reference collimator. These developments, together with the present results, provide a theoretical basis and a quantitative framework for optimizing infrared collimators used in high-accuracy single-channel flight vehicle testing.

REFERENCES

[1]. L. Xiao, Y. Xie, *"An Accurate Analytical Method to Determine the Range of Quiet Zone in Compact Antenna Test Range,"* IEEE Transactions on Instrumentation and Measurement, vol. 73, pp. 1-8, (2024).

[2]. P. Huo, Z. Li, J. Wu and M. Bai, *"Pattern Correction From Nonideal Compact Antenna Test Range Measurement,"* IEEE Antennas and Wireless Propagation Letters, vol. 23, no. 6, pp. 1660-1664, (2024).

[3]. B. Fu, P. Huo, J. Wu and Z. Li, *"Concave Serrated-Edge Reflectors for Compact Range With Lower Frequency Limit,"* IEEE Transactions on Antennas and Propagation, vol. 73, no. 4, pp. 2147-2159, (2025).
[4]. D. Jung et al., *"Development of linear astigmatism free confocal off-axis reflective collimator for automatic alignment device for aviation,"* Proc. SPIE, (2024).
[5]. M. Tecza et al., *"HARMONI & ELT: prototyping and testing the spectrograph TMA collimator alignment procedure,"* Proc. SPIE, (2024).
[6]. T. Hirasawa et al., *"Photoacoustic microscopy for real-time monitoring of near-infrared optical absorbers inside biological tissue,"* J. Biomed. Opt., (2024).
[7]. M. Dirix and S. F. Gregson, *"Design Effects of the Junction Contour of a Blended Rolled Edge Compact Range Reflector,"* Proc. 18th European Conference on Antennas and Propagation (EuCAP 2024), Glasgow, UK, pp. 1–5, (2024).
[8]. Q. Hu and C. Liu, *"Two-dimensional electromagnetic scattering analysis based on the boundary element method,"* Frontiers in Physics, vol. 12, art. 1424995, (2024).
[9]. N. Chopra and J. Lloyd-Hughes, *"Optimum optical designs for diffraction-limited terahertz spectroscopy and imaging systems using off-axis parabolic mirrors,"* Journal of Infrared, Millimeter, and Terahertz Waves, vol. 44, no. 11–12, pp. 1015–1037, (2023).
[10]. D. Cabornero, L. Lozano, I. González, Á. Somolinos, and F. Cátedra, *"Application of Relational Databases to the Acceleration of Ray Tracing in High Frequency Asymptotic Techniques,"* IEEE Open Journal of Antennas and Propagation, (2025).
[11]. C. Shi, S. Liang, X. Gu, J. Pan, and L. Zuo, *"Hybrid Method of Moments and Generalized Scattering Matrix: Applications to Antennas in Radomes, Reflectors, and Implantable Media,"* arXiv preprint arXiv:2509.22000, (2025).
[12]. Боголюбов А.Н., Боголюбов Н.А., Свешников А.Г., *"Физические основы приборостроения,"* Vol.2, No.1, C. 10, (2013).
[13]. Свешников А.Г., Могилевский И.Е., *"Математические задачи теории дифракции,"* Москва., (2010).
[14]. Le Vu Nam, Pham Dinh Quy, Nguyen Thu Cam, *"Design of cooled MWIR continuous zoom optical systemforlong-range surveillance,"* Journal of Military Science and Technology, vol. 105, pp. 98-105, (2025).
[15]. Lai Thanh Tuan, Dang Thanh Dat, Nguyen Thai Dung, *"Design and optimization of axial length in a -1× magnificationimage-inverting optical system,"* Journal of Military Science and Technology, vol. 107, pp. 87-94, (2025).

TÓM TẮT

Xây dựng mô hình toán và đánh giá ảnh hưởng của mép bo tròn gương parabol tới chất lượng trường chuẩn trực của ống chuẩn trực hồng ngoại sử dụng trong thiết bị kiểm tra thiết bị bay một kênh

Bộ chuẩn trực hồng ngoại (IR) sử dụng gương parabol được sử dụng rộng rãi trong các hệ thống thử nghiệm thiết bị bay một kênh nhằm tạo ra trường bức xạ gần như sóng phẳng. Tuy nhiên, hiện tượng nhiễu xạ tại mép gương làm suy giảm độ đồng đều của trường bức xạ và hạn chế độ chính xác của phép đo. Bài báo này trình bày mô hình toán học của bộ chuẩn trực hồng ngoại sử dụng gương parabol có mép bo tròn nhằm đánh giá ảnh hưởng của hình dạng mép gương đến trường bức xạ. Mô hình được xây dựng trên cơ sở phương trình Helmholtz hai chiều và được giải bằng phương pháp phương trình tích phân biên để xác định phân bố dòng điện cảm ứng trên bề mặt gương cũng như trường bức xạ trong vùng làm việc. Kết quả mô phỏng số cho thấy mép gương bo tròn có khả năng giảm hiệu quả các gợn biên độ do nhiễu xạ gây ra và cải thiện đáng kể độ đồng đều của trường bức xạ so với gương có mép sắc truyền thống. Mô hình đề xuất cung cấp cơ sở lý thuyết cho việc tối ưu hóa thiết kế bộ chuẩn trực hồng ngoại sử dụng gương parabol phục vụ các hệ thống thử nghiệm thiết bị bay một kênh có độ chính xác cao.

Từ khoá: Ống chuẩn trực hồng ngoại; Gương parabol; Mép bo tròn; Nhiễu xạ mép; Thiết bị bay một kênh.